Supporting Information

Cooperative catalysis of $Zn_3(VO_4)_2$/$Ni(OH)_2$/rGO nanosheet arrays advancing highly active O_2 reduction

Xue Li[a], Xinglong Gao[a], Enyan Guo[a], Mingzhi Wei[a], Conghui Si[a], Qifang Lu[a*], Yingping Pang[b*]

[a]State Key Laboratory of Biobased Material and Green Papermaking, Qilu University of Technology (Shandong Academy of Sciences), Jinan 250353, P. R. China

[b]Key Laboratory of Colloid and Interface Chemistry, Ministry of Education, School of Chemistry and Chemical Engineering, Shandong University, Jinan 250100, P. R. China

Tel: 86-531-89631227

Fax: 86-531-89631227

[*] Author to whom correspondence should be addressed. E-mail: luqf0110@126.com (Q. F. Lu)
[*] Author to whom correspondence should be addressed. E-mail: yppang@sdu.edu.cn (Y. P. Pang)

1. Experimental section

1.1 Synthesis of $Zn_3(VO_4)_2$ nanosheets

In a typical synthesis, 0.656 g of 2-methylimidazole was dissolved in 25 mL of methanol. Then, the solution was slowly poured into 25 mL of methanol solution containing 0.22 g of $Zn(CH_3COO)_2 \cdot 2H_2O$ under continuous stirring. Next, the mixture solution was stirred at room temperature for 120 min before aging overnight. Finally, the obtained ZIF-8 rhombic dodecahedrons were washed with ethanol three times and dried at 60 °C overnight.

0.034 g of ZIF-8 and 0.012 g of NH_4VO_3 were dissolved in 30 mL of deionized water. Then, the mixed solution was transferred into a 50 mL Teflon-lined stainless-steel autoclave and kept at 120 °C for 6 h. Next, the precursor was collected by centrifugation, washed with ethanol three times, and dried overnight. Finally, the as-prepared precursor was pyrolyzed in a tube furnace at 300 °C for 2 h with a heating rate of 2 °C min^{-1}. After naturally cooling down to room temperature, the $Zn_3(VO_4)_2$ nanosheets were obtained and used without any further treatment.

1.2 Synthesis of $Zn_3(VO_4)_2$/$Ni(OH)_2$ nanosheets

0.01 g of $Zn_3(VO_4)_2$, 0.12 g of $NiCl_2 \cdot 6H_2O$, and 0.15 g of urea were dissolved in 30 mL of deionized water. Then, the mixed solution was transferred into a 50 mL Teflon-lined stainless-steel autoclave and kept at 95 °C for 12 h. After naturally cooling down to room temperature, the $Zn_3(VO_4)_2$/$Ni(OH)_2$ nanosheets were collected by centrifugation, washed with ethanol three times, and dried at 60 °C for 12 h.

1.3 Synthesis of $Zn_3(VO_4)_2$/$Ni(OH)_2$/rGO nanosheets

Firstly, 50 mg of GO (Aladdin, China) was transferred into a crucible and then heated at 350 ℃ for 2 h in a muffle furnace. Then, 30 mg of rGO was added to 10 mL of deionized water, before adding 30 mg of $Zn_3(VO_4)_2/Ni(OH)_2$. After stirring for 30 min, the mixed solution was sonicated for 1 h. Finally, the $Zn_3(VO_4)_2/Ni(OH)_2$/rGO were collected by centrifugation, washed with ethanol three times, and dried at 60 °C for 12 h.

2. Materials characterization

XRD patterns were collected on a Bruker D8 Advance powder X-ray diffractometer (2D detector) using Cu Kα radiation (λ = 0.15406 nm) at an operating voltage and current of 40 kV, and 40 mA, respectively. The XRD pattern processing was conducted on Jade Analysis software (v. 9). Bright-field TEM observations were performed on a JEOL JEM-2100F transmission electron microscope at an acceleration voltage of 200 kV. SEM images were acquired on a Hitachi S-520 electron microscope with a secondary electron detector at an acceleration voltage of 3 kV. XPS data were obtained on an ESCALAB 250Xi spectrometer, using a monochromatic Al Kα radiation (1486.68 eV) at a custom-designed ultrahigh-vacuum system with a base pressure lower than 10^{-9} Pa. All XPS spectra were calibrated by shifting the detected C 1*s* peak to 284.8 eV. The XPS data were processed using Avantage software (FWHM, L/G Mix, Tail Mix, Tail Height, and Tail Exponent). AFM was carried out in tapping mode with a Veeco-Bruker Multimode 8 equipped with an ultrasharp cantilever with a diamond-like carbon tip (NSG01, NT-MDT)

under ambient conditions. The image was flattened using the NanoScope Analysis software (v. 1.40).

3. Electrochemical measurement

The electrochemical performance was assessed on a CHI 760e electrochemical workstation (Chenhua, China) equipped with a typical three-electrode system. Pt wire and Hg/HgO were used as the counter electrode and reference electrode, respectively. The working electrode was prepared by drop-coating catalyst ink on the polished glassy carbon (GC) electrode with a diameter of 5.0 mm (geometric surface area, 0.196 cm^2). The catalyst ink was a mixture of 4.0 mg of sample, 4.0 mg of conductive carbon, and 40 μL of Nafion solution (5 wt%) dispersed in 750 μL of isopropanol solvent and 250 μL deionized water. To form a homogeneous dispersion, the catalyst ink was ultrasonically treated for 1 h. 10 μL of the ink was then transferred onto the GC electrode and dried in a vacuum tank at room temperature for 6 h, yielding a catalyst mass loading of 0.20 mg cm^{-2}. All measured potentials were converted to RHE with the Nernst equation. For ORR tests, the polarization curves were recorded in an O_2-saturated 0.1 M KOH electrolyte. Electrochemical impedance spectroscopy (EIS) was conducted at open potential with frequencies from 0.01 to 100,000 Hz. Accelerated durability tests of catalysts were performed by continuous potential cycling between -0.5 and 0 V versus Hg/HgO at a scan rate of 100 mV s^{-1} for 3000 cycles. CV method was used to measure the electrochemical double-layer capacitance (C_{dl}). The potential was swept at different scan rates of 20, 40, 60, 80, 100, and 120 mV s^{-1}. The halves of the positive and negative current density differences at the

center of the scanning potential range were plotted versus scan rates where the slopes represent the double-layer capacitance. The overall water splitting tests were performed in a two-electrode system with catalysts loaded on Ni foam (mass loading: 0.4 mg cm^{-2}). Polarization curves were obtained using LSV with a scan rate of 5 mV s^{-1}. The chronopotentiometry tests were conducted at a constant current density of 10 mA cm^{-2} for 48 h.

The ORR kinetics of the prepared catalyst was studied with the rotating disk electrode (RDE) measurement. The transferred electron number (n) was calculated via the Koutecky-Levich (K-L) equations:

$$1/J = 1/J_L + 1/J_K = 1/B\omega^{1/2} + 1/J_K \quad (1)$$

$$B = 0.62nFkD_0^{2/3}\nu^{-1/6}C_0 \quad (2)$$

$$J_K = nFkC_0 \quad (3)$$

in which J, J_K, and J_L correspond to the measured current density, the kinetic current density, and the diffusion-limiting current density, respectively. B is a constant as a function of the concentration, diffusion coefficient of O_2 in the electrolyte, and viscosity of the electrolyte; n is the transferred electron number; F is the Faraday constant (96485 C mol^{-1}); D_0 is the diffusion coefficient of O_2 in the 0.1 M KOH solution (1.9×10^{-5} cm^2 s^{-1}); ω is the angular velocity of the disk (ω=2πN, N is the linear rotation speed); ν is the kinetic viscosity of the electrolyte (0.01 cm^2 s^{-1}); C_0 is the bulk concentration of O_2 (1.2×10^{-6} mol cm^{-3}); k is the electron transfer rate constant.

4. Theoretical calculations

All DFT calculations in our work were carried out using the Vienna Ab-initio simulation package (VASP). The exchange and correlation effects were described by the generalized gradient approximation (GGA) with PW91. An energy cut of 450 eV was used to expand the Kohn-Sham wave functions. All the geometry structures and atomic positions were fully relaxed by a conjugate gradient (CG) method with convergence criteria of 0.01 eV $Å^{-1}$ and 10^{-5} eV $atom^{-1}$ for force and energy, respectively. The irreducible Brillouin zones were sampled with 3×3×1 k-points. In calculation, the geometry models were firstly optimized via VASP, and then their electronic structures and free energy were calculated.

The free energy (ΔG) was obtained from

$$\Delta G = \Delta E + ZPE - T\Delta S + ne\Delta U \quad (4)$$

where ΔE is the total energy; ZPE represents the zero-point energy; the entropy (ΔS) of each adsorbed state is yielded from DFT calculation; n is the electron number of such state; e is the elementary charge, ΔU refers to the applied electrode potential.

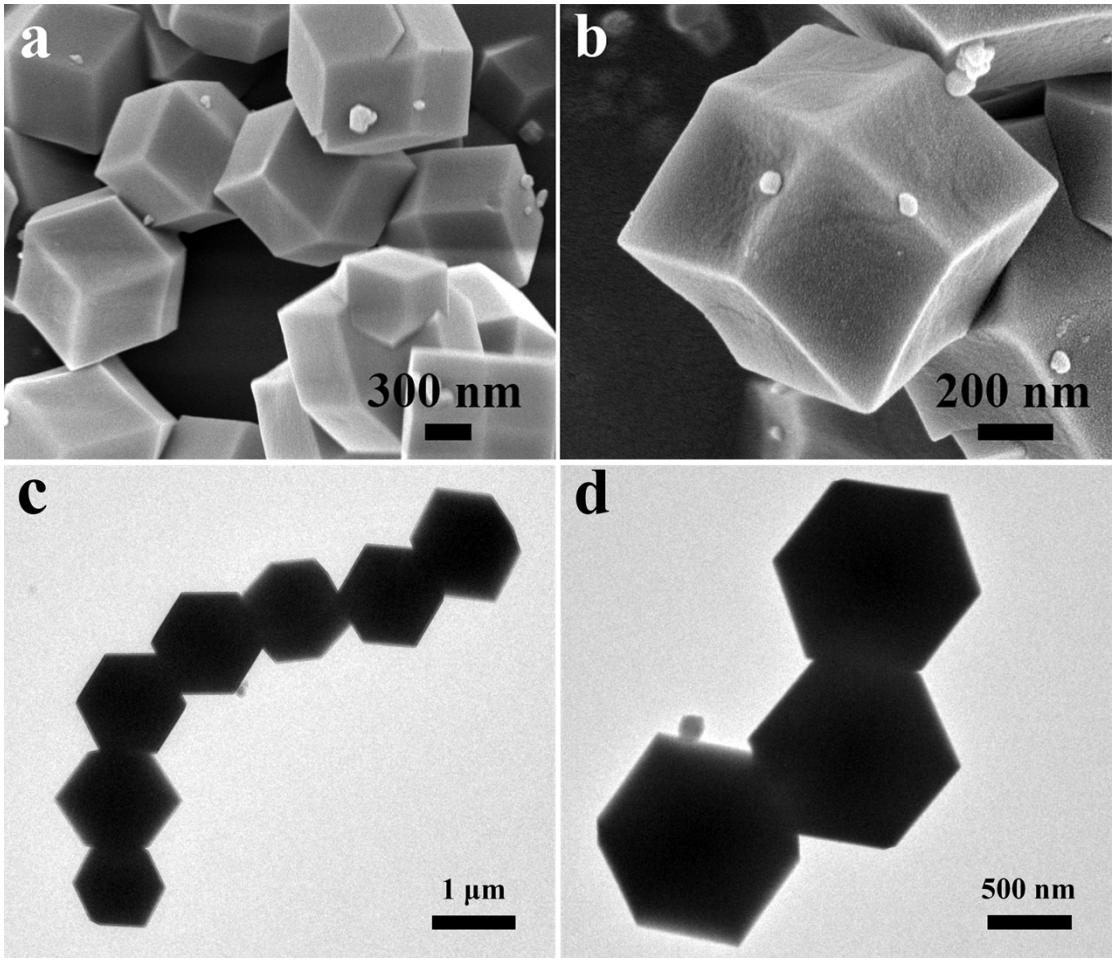

Fig. S1 (a, b) SEM, and (c, d) TEM images of ZIF-8.

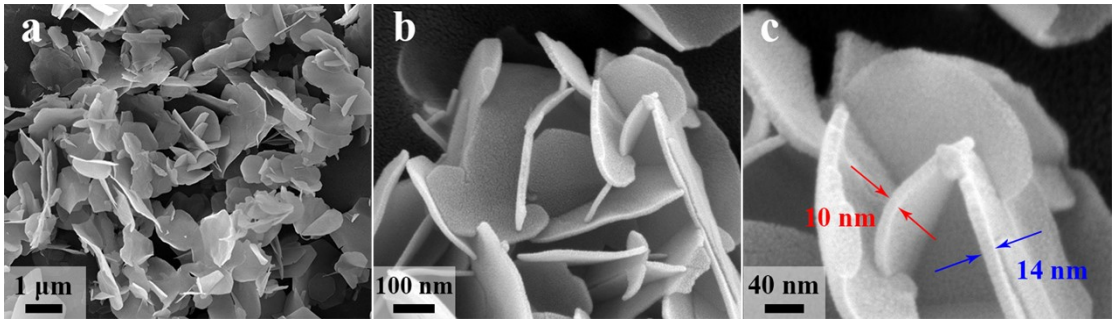

Fig. S2 SEM images of $Zn_3(VO_4)_2$ nanosheets at different magnifications.

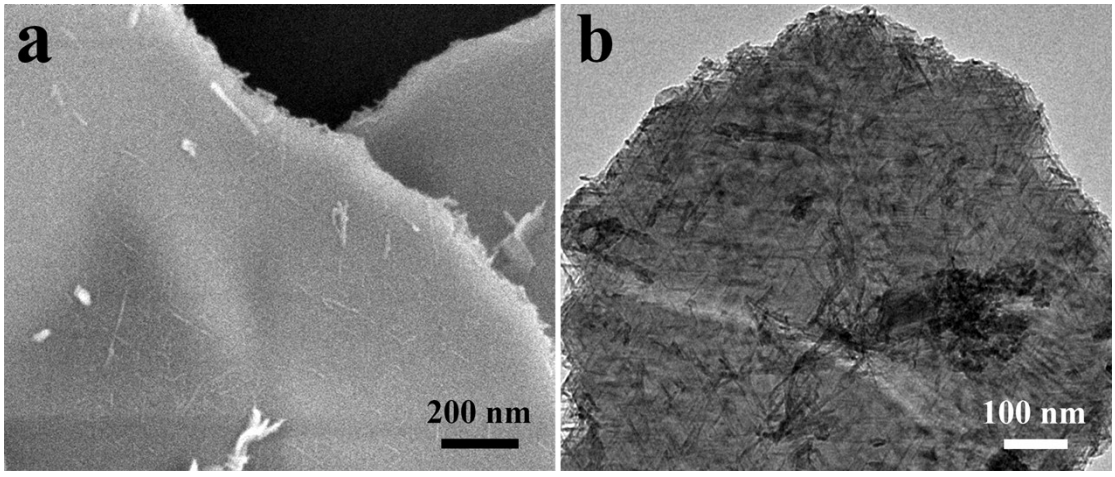

Fig. S3 (a) SEM, and (b) TEM images of $Ni(OH)_2$ nanosheets.

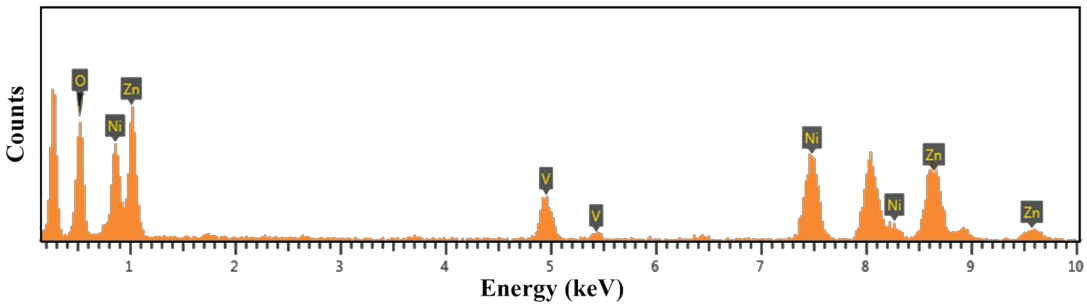

Fig. S4 TEM-EDS spectrum of $Zn_3(VO_4)_2/Ni(OH)_2$ nanosheets.

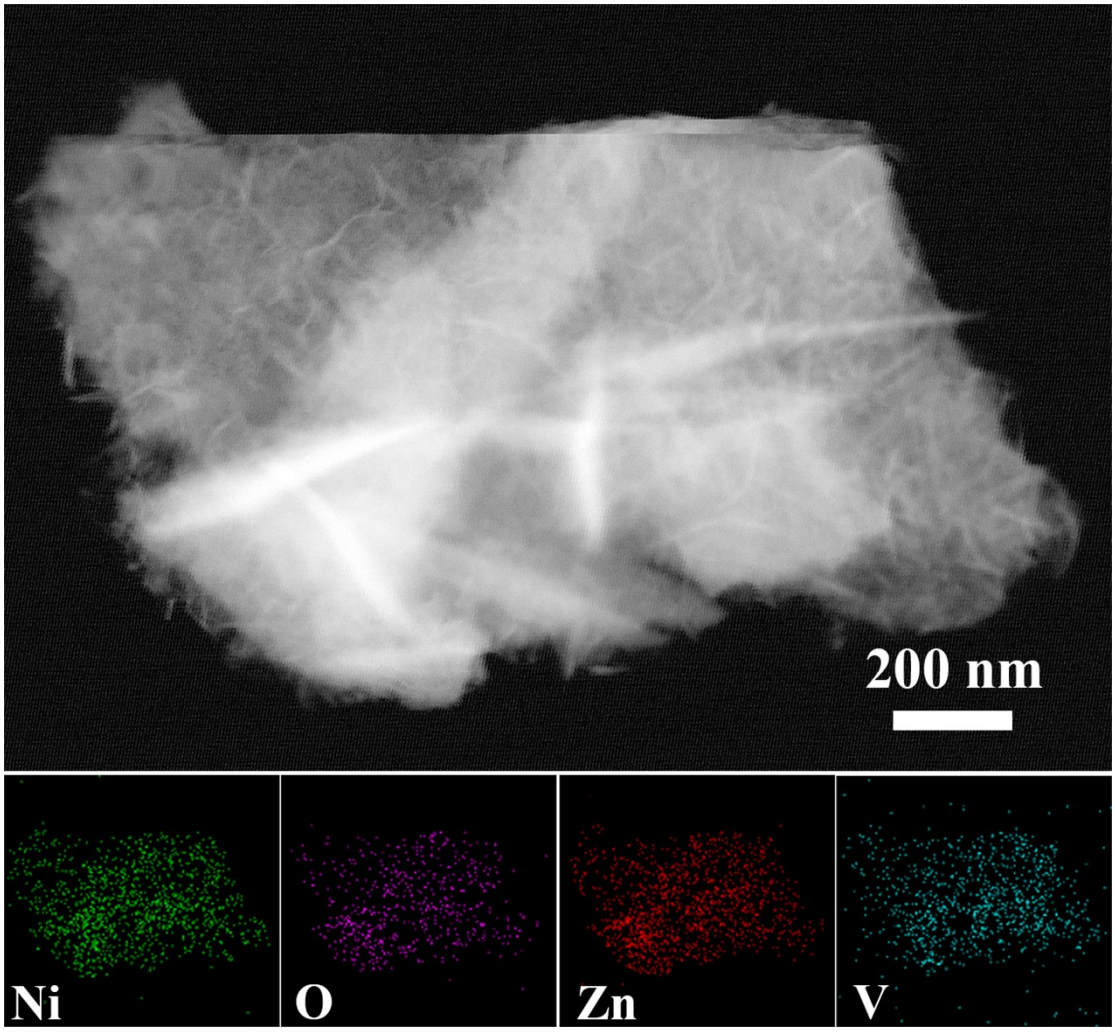

Fig. S5 EDS elemental mapping images of $Zn_3(VO_4)_2/Ni(OH)_2$ nanosheets.

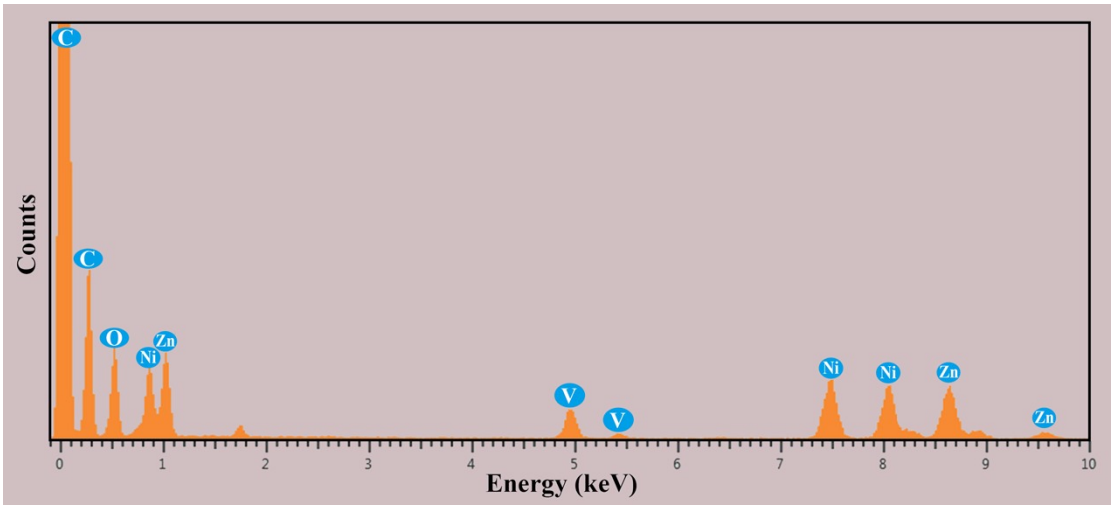

Fig. S6 TEM-EDS spectrum of $Zn_3(VO_4)_2$/$Ni(OH)_2$/rGO nanosheets.

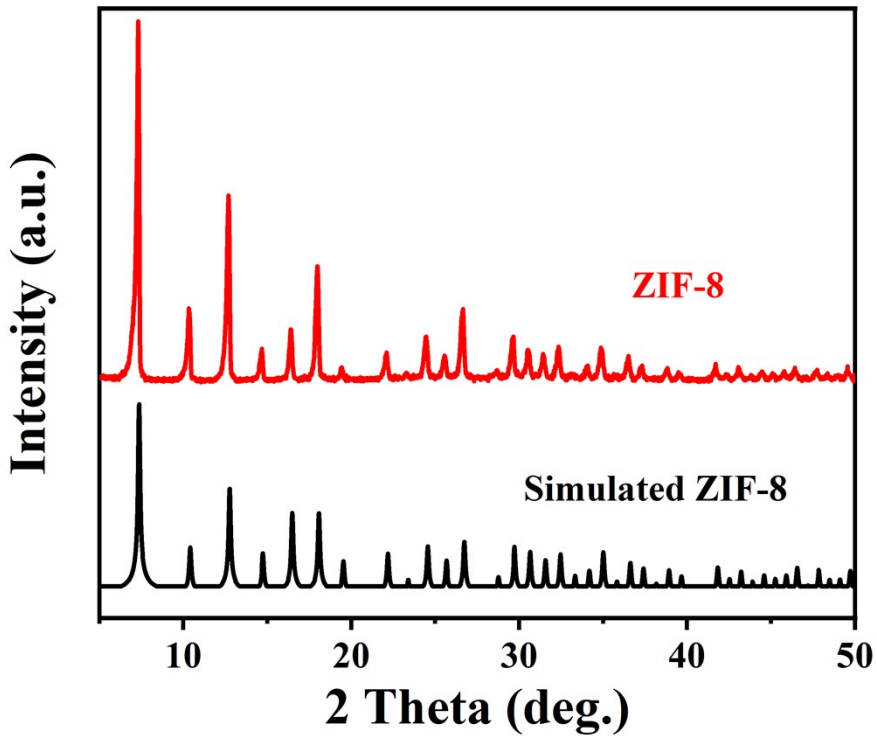

Fig. S7 XRD pattern of pristine ZIF-8.

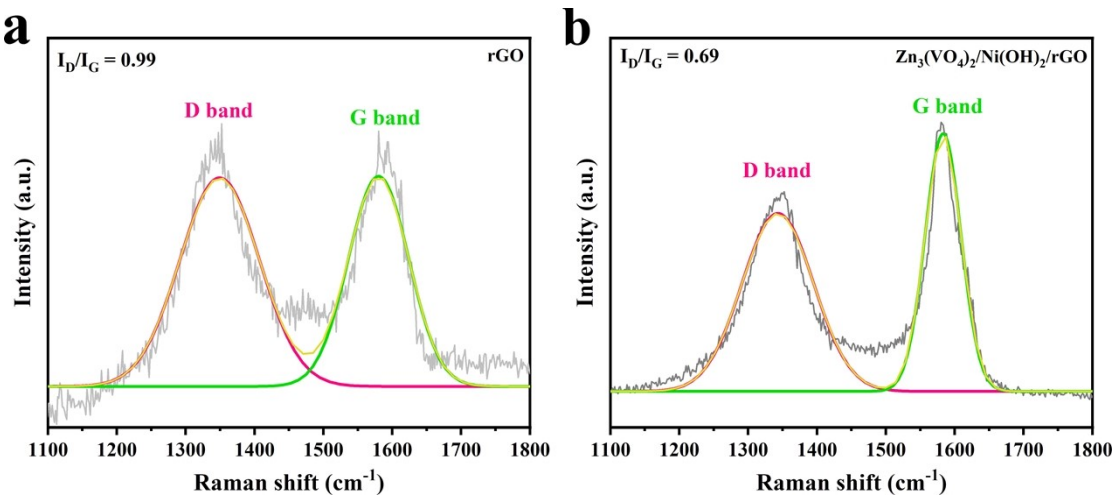

Fig. S8 Raman spectra of rGO and $Zn_3(VO_4)_2/Ni(OH)_2$/rGO nanosheets.

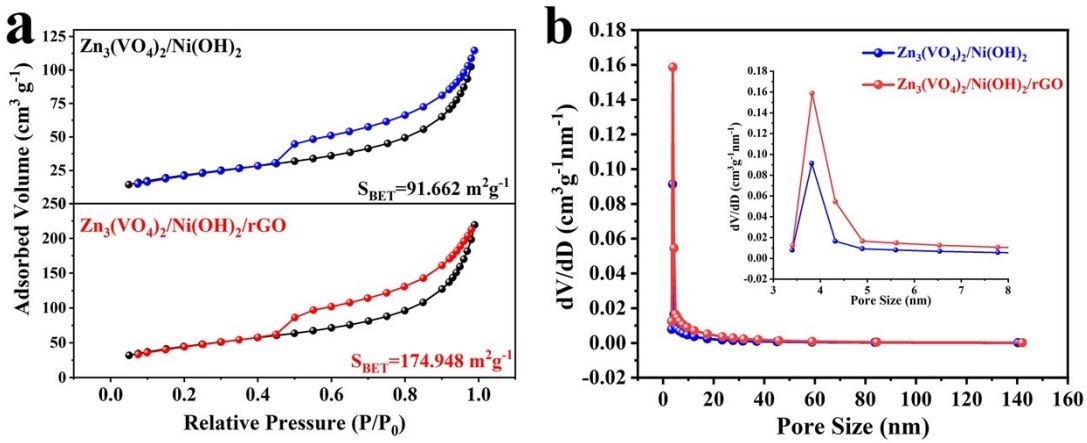

Fig. S9 (a) Nitrogen adsorption-desorption isotherms and (b) pore size distribution of the $Zn_3(VO_4)_2/Ni(OH)_2$ and $Zn_3(VO_4)_2/Ni(OH)_2$/rGO nanosheets.

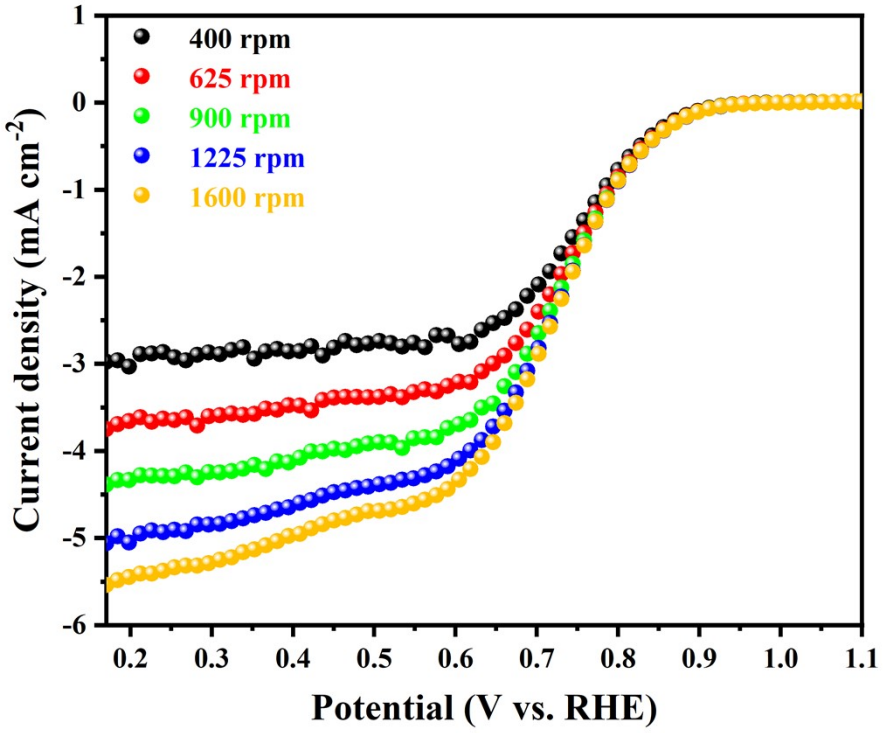

Fig. S10 LSV curves at various rotation rates of $Zn_3(VO_4)_2/Ni(OH)_2$/rGO nanosheet arrays in the ORR process.

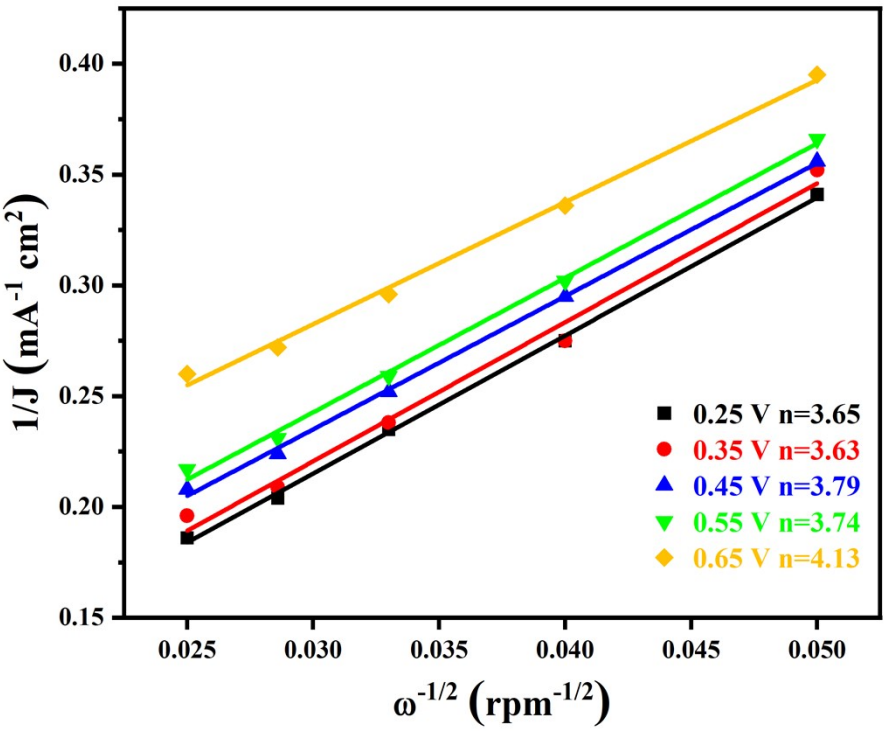

Fig. S11 K-L plots at potentials of 0.65, 0.55, 0.45, 0.35, and 0.25 V vs. RHE of $Zn_3(VO_4)_2/Ni(OH)_2$/rGO nanosheet arrays.

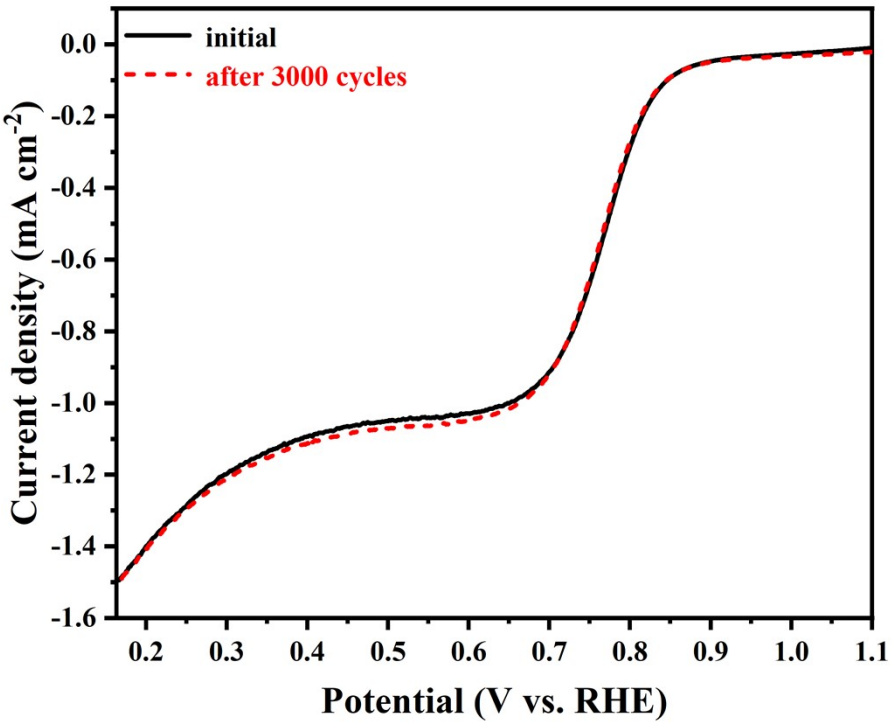

Fig. S12 ORR polarization curves of $Zn_3(VO_4)_2/Ni(OH)_2$/rGO catalyst initially and after 3000 cycles in 0.1 M KOH.

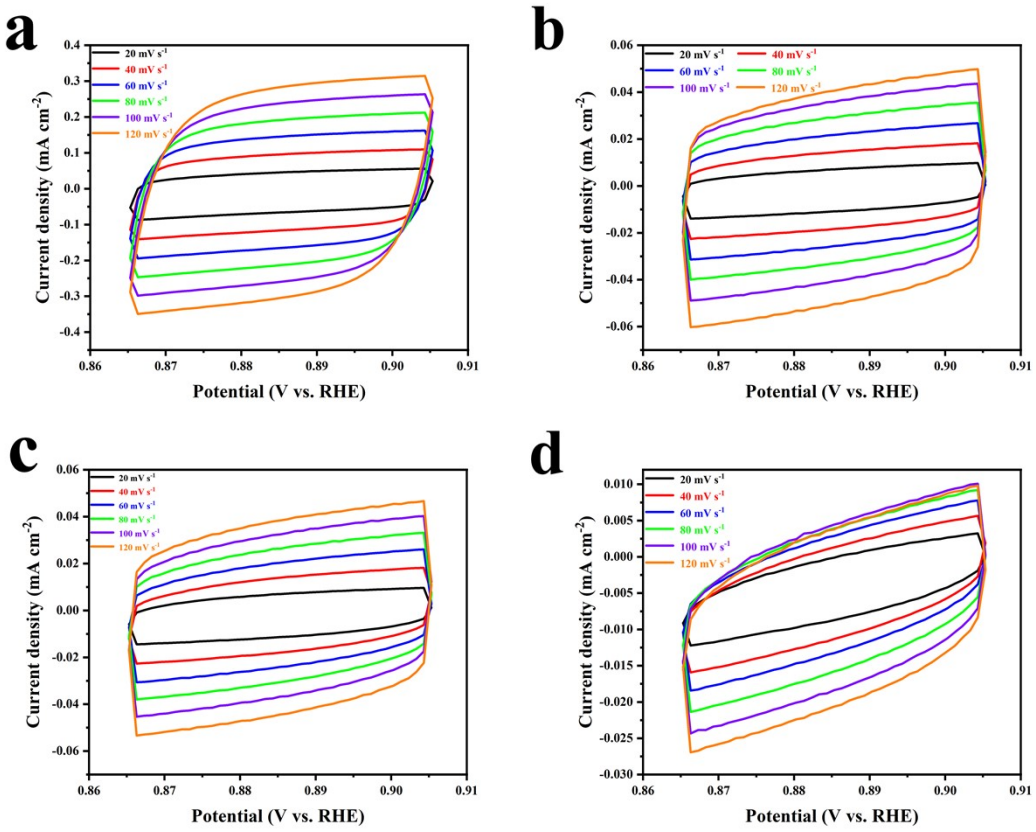

Fig. S13 Typical CVs in a non-faradic potential region of (a) $Zn_3(VO_4)_2/Ni(OH)_2$/rGO, (b) $Zn_3(VO_4)_2/Ni(OH)_2$, (c) $Ni(OH)_2$, and (d) $Zn_3(VO_4)_2$ catalysts in 0.1 M KOH.

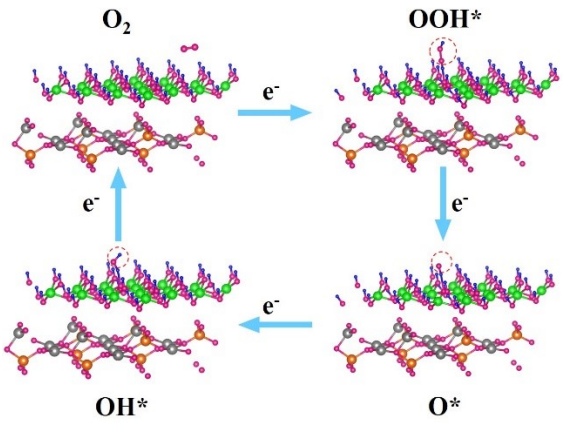

Fig. S14 The ORR reaction pathway in alkaline solution.

Table S1. ORR and OER performance of different electrocatalysts.

Catalysts	Electrolyte solution	$E_{1/2}$ (V vs. RHE)	OER overpotential (mV)	ORR Tafel slope (mV dec^{-1})	OER Tafel slope (mV dec^{-1})	Ref.
$Co_3V_2O_8$	1 M KOH	-	318	-	130	[1]
Fe doped MOF	KOH	0.75	220	105	59	[2]
CoV@CoO		(0.1 M KOH)	(1 M KOH)	(0.1 M KOH)	(1 M KOH)	
$Co_3V_2O_8$	1 M KOH	-	510	-	-	[3]
$Ni_3V_2O_8$ NCs	1 M KOH	-	398	-	164	[4]
COV500	1 M KOH	-	340	-	127	[5]
Co_2VO_4	1 M KOH	0.83	-	59	-	[6]
$Co_3V_2O_8$	1 M KOH	-	359	-	65	[7]
Au/VOx	1 M KOH		360		98	[8]
$Zn_3(VO_4)_2/Ni(OH)_2$ /rGO	0.1 M KOH	0.83	510	79.3	77	This work

Table S2. R_s and R_{ct} of different samples.

Samples	R_s (ohm)	R_{ct} (ohm)
$Zn_3(VO_4)_2$	6.327	19424
$Ni(OH)_2$	2.767	21218
rGO	3.874	943.9
$Zn_3(VO_4)_2/Ni(OH)_2$	3.372	1789
$Zn_3(VO_4)_2/Ni(OH)_2$/rGO	3.882	78.24

References

[1] Z. Yang, H. Chen, M. Xiang, C. Yu, J. Hui and S. Dong, Int. *J. Hydrogen Energ.*, 2022, **47**, 31566-31574.

[2] A. Muthurasu, A.P. Tiwari, K. Chhetri, B. Dahal and H.Y. Kim, *Nano Energy*, 2021, **88**, 106238.

[3] A. Mondal, S. Ganguli, H.R. Inta and V. Mahalingam, *ACS Appl. Energ. Mater*., 2021, **4**, 5381-5387.

[4] S.S. Sankar, K. Karthick, K. Sangeetha, R.S. Gill and S. Kundu, *ACS Sustain. Chem. Eng.*, 2020, **8**, 4572-4579.

[5] G.M. Thorat, H.S. Jadhav, A. Roy, W.-J. Chung and J.G. Seo, *ACS Sustain. Chem. Eng.*, 2018, **6**, 16255-16266.

[6] C. Mu, J. Mao, J. Guo, Q. Guo, Z. Li, W. Qin, Z. Hu, K. Davey, T. Ling and S.Z. Qiao, *Adv. Mater.*, 2020, **32**, 1907168.

[7] M. Xing, L.-B. Kong, M.-C. Liu, L.-Y. Liu, L. Kang and Y.-C. Luo, *J. Mater. Chem. A*, 2014, **2**, 18435-18443.

[8] B. Das, M. Sharma, A. Hazarika and K.K. Bania, *ChemistrySelect*, 2019, **4**, 7042-7050.